ADVANCED ENGINEERING MATERIALS
www.aem-journal.com

Directed Energy Deposition versus Wrought Ti-6Al-4V: A Comparison of Microstructure, Fatigue Behavior, and Notch Sensitivity

Seyed Mohammad Javad Razavi and Filippo Berto*

Laser Engineered Net Shaping (LENS), a Direct Energy Deposition (DED) additive manufacturing process is a 3D manufacturing process generally used to produce fully dense parts or to repair/add additional material to an existing component. The main aim of this work is to evaluate the fatigue behavior of LENS specimens in the presence of geometrical discontinuities and to compare its performance to the one obtained from wrought specimens. For this aim, axial fatigue tests are carried out on three sets of specimens namely, smooth, semi-circular and V-notched specimens to determine the fatigue strength and notch sensitivity of the LENS and wrought Ti-6Al-4V materials. The LENS material shows higher fatigue strength and notch sensitivity compared to wrought material which is attributed to the unique microstructural features leading to different fatigue failure mechanisms. Further, the fatigue data is assessed by use of strain energy density as a failure criterion.

1. Introduction

Additive Manufacturing (AM) technology is a process that enables the manufacturing of unprecedented complex designs in an economic fashion produced layer-by-layer by using a combination of energy delivery and material deposition. AM parts are commonly no longer isotropic, mostly including residual stresses, occasionally not fully dense, having rough surfaces and there is a high chance of internal defects (e.g., trapped voids, lack of fusion between the layers, etc.), which are all dependent on the underlying manufacturing strategy related to the input geometry. Different post treatment strategies have been proposed by researchers to overcome these challenges. Among the common suggested methods for improving the mechanical performance of AM parts are the application of heat-treatment for releasing the residual stresses, surface treatments (i.e., sand blasting, shot peening, chemical etching) for reducing the surface roughness, Hot Isostatic Pressing (HIP) for reducing the internal porosities, and machining the AM parts for improving the surface roughness and eliminate the sub-surface defects.

Direct Energy Deposition (DED) includes all the processes where focused energy generates a melt pool into which feedstock is deposited. Among different DED methods, LENS is one of the most commercialized forms that uses metal powder injection into a molten pool created by a focused, high-powered laser beam (see **Figure 1**).[1,2] This technology can be utilized for the AM fabrication of a wide range of alloys such as stainless steel, aluminum, and titanium as well as metal matrix composites and functionally graded materials. The main applications for LENS technology in aerospace industries include the repair and overhaul of worn and cracked components without the need to replace the whole component. The overall cost and required time for repairing components using LENS technology was reported to be significantly less than other repair methods. Flawless metallurgical bonding between the LENS-added material and the base material results in promising mechanical performance of the LENS repaired parts compared to the mechanically bonded repairs using thermal spray or chroming processes or even conventional welding processes. This technology is also being used for rapid prototyping, rapid manufacturing, and limited-run manufacturing for aerospace, defense, and medical industries.[3–9]

High production rate and the negligible porosity of LENS parts have resulted in common application of this process for the production of industrial parts, however, the reported range of surface roughness in LENS components is higher than the other AM method. While the surface roughness of selective laser melting (SLM) and electron beam melting (EBM) components is respectively $R_a = 5$–$15\,\mu m$ and $20\,\mu m$, LENS components have a surface roughness range of $R_a = 10$–$91\,\mu m$.[8] Hence, the post-process for improving the surface roughness and shaping of fine details by machining, grinding or polishing has been required to overcome this inherent limitation of LENS method.[10,11]

Among different titanium alloys, Ti-6Al-4V has been widely used both for biomedical applications and critical industrial applications due to its high specific strength, corrosion resistance, and fatigue strength. Numerous studies have

S. M. J. Razavi, Prof. F. Berto
Department of Mechanical and Industrial Engineering
Norwegian University of Science and Technology (NTNU)
Richard Birkelands vei 2b, 7491 Trondheim, Norway
E-mail: javad.razavi@ntnu.no

DOI: 10.1002/adem.201900220

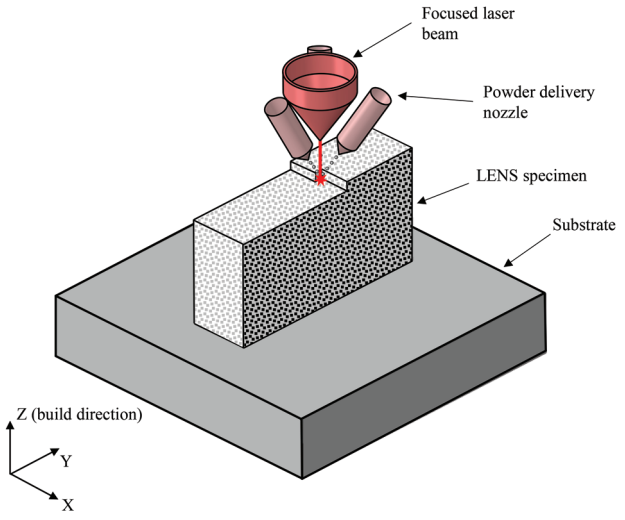

Figure 1. A Schematic illustration of LENS process.

evaluated the microstructure and mechanical properties of Ti-6Al-4V produced by LENS technique.[12–21] Due to cyclic heating induced by sintering the new layers followed by fast cooling during the LENS process, complex microstructural features, including large columnar prior β grains, fine α + β basketweave morphology, and in some cases martensite α' phase were observed. Comparable yield and tensile strengths and lower ductility were found compared to that of the wrought material.

Dealing with high cycle fatigue (HCF) behavior of LENS components, initial researches reported shorter fatigue lives were reported for the LENS Ti-6Al-4V compared to the wrought material.[13,22,23] This was attributed to the presence of internal and surface defects within the tested LENS specimens. As reported by Prabhu et al.,[22] eliminating the surface defects in LENS specimens led to longer fatigue lives that exceed the lower survival probability band of fatigue lives reported for wrought annealed material and lies in the upper survival probability band of hot isostatic pressed (HIP) casted material. In another research by Bian et al.,[23] it was observed that subjecting the LENS specimens to HIP process reduces the effect of internal pores, enhancing the fatigue strength to the same range as wrought material. Amsterdam and Kool[24] observed similar HCF fatigue behavior for wrought and severely porous LENS Ti-6Al-4V specimens, indicating that a fatigue strength higher than that of wrought material can be achieved for porosity-free LENS components. This was later shown in a research by Razavi et al.,[25] where they obtained higher fatigue strengths for porosity-free LENS Ti-6Al-4V alloy compared to the wrought material. The inconsistency in the reported fatigue behavior of LENS Ti-6Al-4V may be attributed to different employed process parameters and post treatments, which consequently led to different microstructures and porosity levels in the produced parts. The thermal history, microstructure, residual stress level and morphology of the pores strongly depends on manufacturing process parameters, such as laser power, head write speed, layer height, hatch spacing and powder flow rate.[23]

In design of industrial components, the presence of geometrical discontinuities such as notches which induces localized stress gradient is unavoidable. Due to commonly negative effect of notches on fatigue life of mechanical components, it is an essential task to evaluate the resistance of the metallic materials against fatigue crack nucleation from the notch border. The fatigue behavior and notch sensitivity of AM components has been the topic of some recently published articles, where the effect of surface roughness and internal defects on the overall behavior of notched components have been evaluated.[26–31]

Currently, very limited design criteria are presented for AM components considering stress concentration phenomena

Table 1. LENS processing parameters.

	Powder size [μm]	Laser power [W]	Head write speed [m min^{-1}]	Layer height [mm]	Hatch spacing [mm]	Powder flow rate [g min^{-1}]
Current research	44–149	325	0.635	0.508	0.381	1.9
Prabhu et al.[22]	44–149	400	0.635	0.254	0.762	2.4
Nassar et al.[33]	126.8	450	0.635	0.18	0.91	3
Zhai et al.[12,34]	44–149	330	0.6	0.3	0.5	1
Zhai et al.[12,34]	44–149	780	0.8	0.4	1.0	2
Sterling et al.[13]	44–149	350	1.016	0.508	0.508	9.6
Sandgren et al.[14]	44–149	330	0.55	0.3	0.5	1
Wolff et al.[15,35]	44–149	710, 800, 940	0.6	0.95	1.25	7.2
Buciumeanu et al.[36]	32.53	350	0.510, 0.762, 1.014	0.02	0.02	9.36
Kistler et al.[16]	44–149	300	0.636	0.25	0.71	2
Niknam et al.[37]	44–149	206	1.5	0.025	–	60
Niknam et al.[37]	44–149	385	2.4	0.025	–	30

arising from geometrical discontinuities. Additionally, to the best of authors knowledge no fatigue data are presented in technical literature by testing notched components made by LENS technology. Hence, this paper aims to contribute to the fundamental understanding of the notch fatigue behavior of Ti-6Al-4V specimens produced by LENS. Three different specimen geometries namely, smooth, semi-circular and V notch were considered for the experimental studies. The notch fatigue behavior of LENS specimens was then compared to that of the wrought Ti-6Al-4V. In the first part of the paper, details of the manufacturing method that was used for fabrication of the samples are described. Afterwards, the microstructures and fatigue test results of smooth and notched LENS specimens are presented and compared to that of the wrought specimens. Lastly, applicability of ASED failure criterion for fatigue life prediction of both LENS and wrought notched specimens was evaluated.

2. Experimental Section

2.1. Specimens Fabrication

Spherical gas atomized Ti-6Al-4V (grade 5) powder with a mesh size of $-100/+325$ (SAE AMS 4998C) provided by TIMET was utilized for LENS fabrication of specimens. An OPTOMEC LENS 850-R machine powered by a 1 kW Nd:YAG laser was utilized for fabrication of 40 cuboid Ti-6Al-4V samples which were fabricated in-series with proper distance to eliminate thermal interaction with the previously deposited specimens. The detailed process parameters are given in **Table 1** together with the process parameters used in the previously published articles on LENS fabrication of Ti-6Al-4V specimens. The 81 mm long specimens were fabricated vertically with a cross-section of 4×16 mm over a mill-annealed Ti-6Al-4V substrate with a thickness of 6 mm.

The substrates were machined after production of the samples. In order to relieve any internal residual stresses, all LENS specimens were stress relieved using annealing heat treatment for one hour in a preheated furnace at 600 °C followed by cooling at room temperature.[32] **Figure 2** illustrates the representative surface morphology of the LENS samples. The LENS samples were ultimately post-machined to eliminate the high surface roughness and sharp valleys on the surface between the sintered layers. A mean surface roughness of 0.25 μm was obtained from all the specimens after machining. The geometry of the test specimens after machining is shown **Figure 3**. Three different geometries including one smooth specimen and two notched specimens namely blunt V-notch and semi-circular were considered for the fatigue test specimens. In order to compare the fatigue behavior of LENS specimens with the conventional Ti-6Al-4V alloys, a set of test specimens with the geometries given in Figure 3 were produced from wrought Ti-6Al-4V. The wrought specimens were machined using the same procedure resulting in similar surface roughness to LENS specimens.

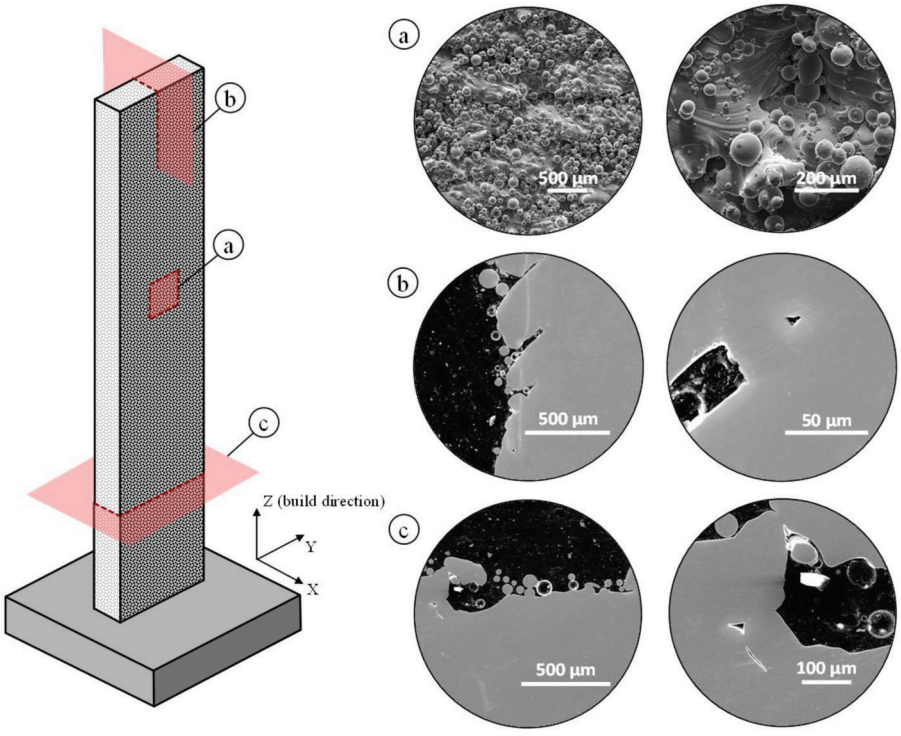

Figure 2. Representative surface condition of the fabricated LENS sample; (a) surface view, (b) longitudinal cross section, and (c) transversal cross section.

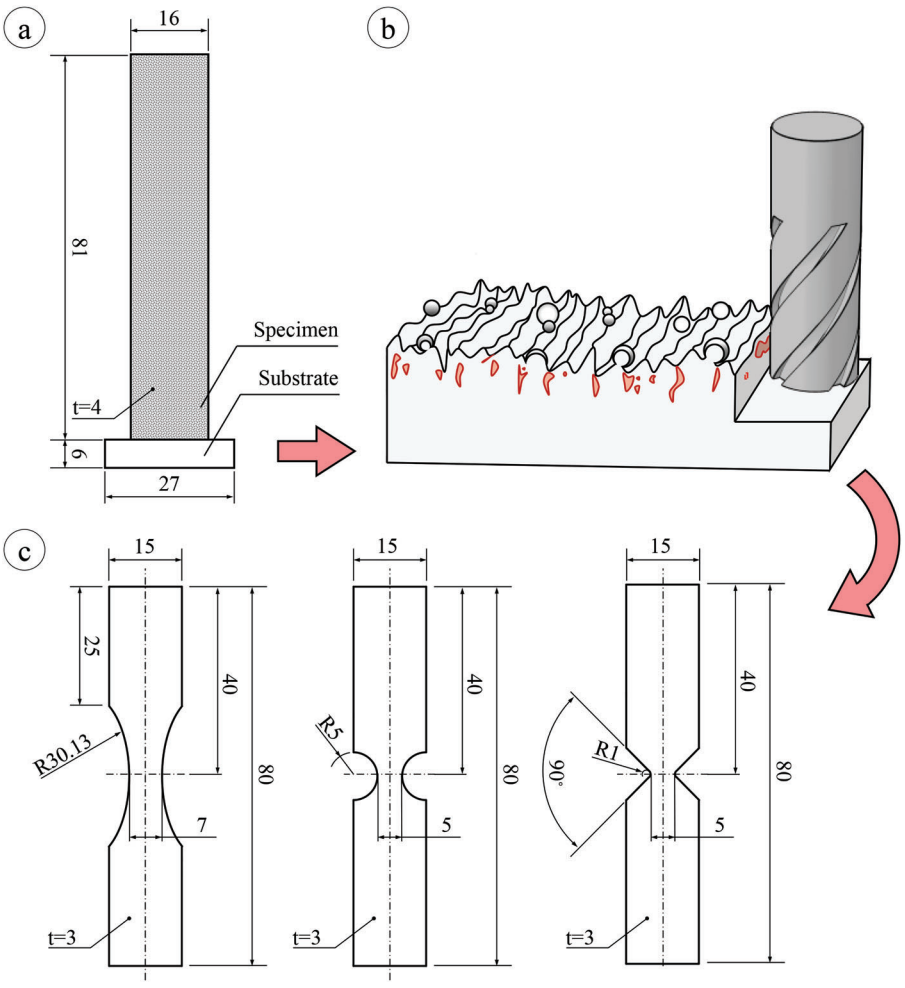

Figure 3. a) geometrical dimensions of the fabricated LENS cuboid, (b) schematic illustration of surface condition and subsurface defect removed by machining, and (c) geometrical dimensions of the fatigue test specimens.

2.2. Microstructural Analysis

Wrought and LENS samples were sectioned horizontally (i.e., x–y plane) and vertically (i.e., x–z and x–y planes) along the centerline to observe the microstructure. The samples were hot-mounted in PolyFast, polished and etched using an etching solution containing 3 ml HF, 6 ml HNO_3 and 100 ml distilled water (ASTM E407-07) also known as Kroll's reagent. The mentioned etchant reveals the α and α' grains of Ti-6Al-4V with white color whereas the β and intergranular β grains have a darker color under optical microscope. The etched samples were then examined using both optical microscope (Olympus, BX53MRF-S, Tokyo, Japan) and scanning electron microscope (SEM) (FEI, Quanta 650 FEG, Oregon, USA) to evaluate the microstructure.

2.3. Fatigue Testing

Specimens were tested under uniaxial fatigue loading using an MTS landmark servohydraulic test machine (Minnesota, USA) equipped with a 50 kN load cell. The tests were performed under load control with a loading ratio of $R = 0.01$ and a frequency of 10 Hz at room temperature. An average of twelve specimens were tested for each testing case to obtain the stress-life curve. Specimens that survived at 5×10^6 cycles were considered as run-out. SEM analysis was performed to observe the fracture surface of tested specimens and define different failure mechanisms in wrought and LENS specimens.

2.4. Theoretical Fatigue Assessment Method

2.4.1. Strain Energy Density Approach

Fundamentals of local failure approaches state that material failure occurs when the key parameter (e.g., stress, strain, strain energy density (SED), etc.) at some critical distance from the geometrical discontinuity reaches a given critical value.[38] Three different methods namely, point method, line method and volumetric method have been investigated in the past considering the values of the key parameter in a single point, averaged on

a line or averaged in a control volume, respectively.[39,40] As one of the common key parameters, strain energy density (SED) has been widely used by numerous researchers for failure assessment of components made of different brittle, quasi-brittle and ductile materials in presence of geometrical discontinuities under static and fatigue loads.[40–42] To the best of authors' knowledge, the first proposal of strain energy density for failure assessment under pure tension and pure compression was dated 1885 by Beltrami.[43] Later on, Sih[44] proposed a point method failure criterion based on SED. Proposing a volumetric SED method, namely average strain energy density (ASED) criterion, Lazzarin and Zambardi[45] stated that failure occurs when the averaged SED value in a control volume around the notch or crack, $\overline{W}$ reaches a material dependent critical value, $W_C = \sigma_t^2/2E$ where σ_t and E are the conventional ultimate tensile strength and the elastic modulus of the material.

The representative control volumes for different notch geometries is illustrated in **Figure 4**, in which 2α is the notch opening angle, ρ is the notch root radius, R_0 is the critical radius, and r_0 is the distance between the notch root and the center of the control volume in blunt notch defined as $r_0 = \rho \times (\pi - 2\alpha)/(2\pi - 2\alpha)$. Dealing with cracks ($2\alpha = 0$, $\rho = 0$) and sharp notches ($\rho = 0$), the control volume is a circle of R_0 radius centered at crack/notch tip. While for the blunt notches under mode I loading, control volume has a crescent shape, with an external radius of $(R_0 + r_0)$ and the maximum width of R_0 as measured along the notch bisector line. The critical radius R_0 under static loading can be calculated using the following equation[45]:

$$R_0 = \frac{(1+\nu)(5-8\nu)}{4\pi}\left(\frac{K_{IC}}{\sigma_t}\right)^2 \tag{1}$$

where ν is the Poisson's ratio and K_{IC} is the fracture toughness of material obtained from pre-cracked specimen.

The average SED value in the control volume for sharp notches under mode I loading can theoretically be calculated using the following equation[45]:

$$\overline{W}_1 = \frac{e_1}{E}\left(\frac{K_1^V}{R_0^{1-\lambda_1}}\right)^2 \tag{2}$$

where e_1 is a function that depends on the notch opening angle 2α, K_1^V is the mode I notch stress intensity factor (NSIF), and λ_1 is the Williams' series eigenvalue.[46] In the case of blunt notches, the average SED value can be analytically expressed as a function of tensile stress at the notch tip under mode I loading[47]

$$\overline{W}_1 = F(2\alpha) \times H\left(2\alpha, \frac{R_0}{\rho}\right) \times \frac{\sigma_{tip}^2}{E} \tag{3}$$

in which F is a function dependent on notch opening angle, H is a function dependent on notch opening angle and the ratio of critical radius to notch root radius (i.e., R_0/ρ) and σ_{tip} is the tensile stress at notch tip.

2.4.2. Synthesis Based on ASED

Lazzarin et al.[45,48] employed the concept of ASED criterion for synthesis of fatigue data obtained by testing different geometries of welded joints. They reported that the average SED in a control volume around the geometrical discontinuities is capable of providing a master curve independent of the geometry of the notch. Having this master curve for each material, one can simply evaluate the fatigue behavior of different notch geometries without the necessity to perform new sets of experiments.

According to the analytical formulation of ASED criterion, the critical radius around the crack and notch tip can be calculated using the fatigue limit of smooth specimens, $\Delta\sigma_A$ (in order to quantify the influence of defects and surface roughness in the material, in the absence of any global stress concentration effect) and the NSIF range at fatigue limit of notched specimens, ΔK_{1A}^V. In this study, the fatigue limit of both smooth and notched specimens was calculated at 10^6 loading cycles.

$$R_0 = \left(\frac{\sqrt{2e_1}\Delta K_{1A}^V}{\Delta\sigma_A}\right)^{\frac{1}{1-\lambda_1}} \tag{4}$$

The ASED range for smooth specimens is defined as $\Delta\overline{W}_1 = \Delta\sigma/2E$, where $\Delta\sigma$ is the stress range in the net section of the test specimens. In the case of the notched specimens under mode I fatigue loading, $\Delta\overline{W}_1$ can be calculated by substituting the NSIF range, ΔK_1^V and notch tip tensile stress range, $\Delta\sigma_{tip}$ in Equations (2) and (3), respectively. As an

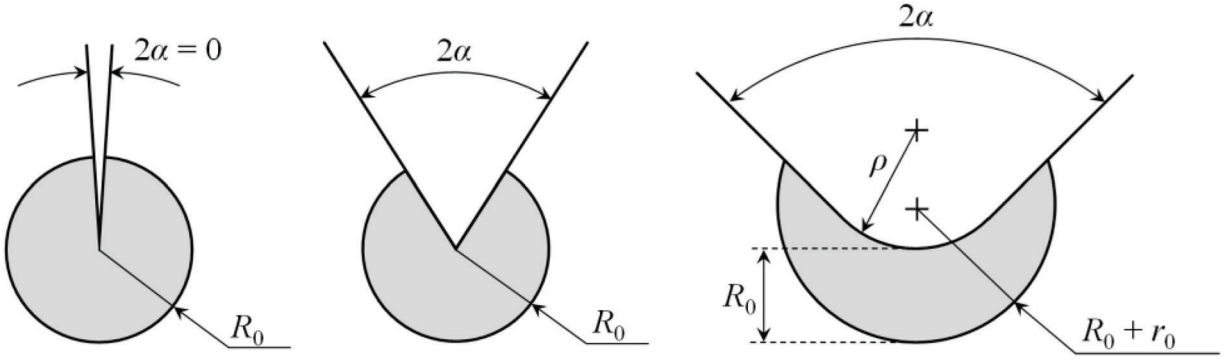

Figure 4. Control volume around crack, sharp V-notch and blunt V-notch under mode I loading condition.[40]

alternative for ASED calculation, one may use finite element software to directly obtain this value by linear elastic analysis of the notched component.

2.4.3. Numerical Analysis

A set of two-dimensional linear elastic analyses was performed in the current research to calculate the stress concentration factor, K_t and SED values of the notched specimens. For this aim, elastic modulus of 110 GPa and Poisson's ratio of 0.34 were used in numerical analyses. Mesh sensitivity analyses were performed on the finite element models considering the opening stress distribution along the notch bisector line as the key parameter in order to obtain the proper element size. A minimum element size of 2 μm was considered for NSIF analysis while a larger element size of 200 μm was considered for the SED analyses. Similar to the previous researches on ASED criterion,[40] independency of the ASED values to the element size was observed in the mesh sensitivity analyses. Double symmetric models were loaded under unit applied stress at the net-sectional area and the peak stress values at the notch root representing the stress concentration factor were obtained. The fatigue notch factor, K_f, was experimentally obtained by dividing the fatigue limit of smooth specimens to that of the notched specimen at 50% probability of survival (i.e., $K_f = \Delta\sigma_{50\%}|\text{smooth}/\Delta\sigma_{50\%}|$ notched). Having the stress concentration factor and fatigue notch factor, one can simply evaluate the notch sensitivity of the material using $q = (K_f - 1)/(K_t - 1)$. According to this formulation, for the material fully sensitive to the presence of notch, $q = 1$ (i.e., $K_f = K_t$), while $q = 0$ represent a material that has fatigue notch factor of $K_f = 1$ meaning that the fatigue limit of notched specimen is equal to that of the smooth one.

3. Results

3.1. Microstructure

A preliminary microstructure investigation by use of optical microscope showed no porosity in both LENS and wrought materials. **Figures 5** and **6** show the microstructures of LENS samples observed using optical microscopy. The optical images in Figures 5 and 6 show the columnar microstructure of the LENS samples with the prior grains elongated along the built direction including three different microstructures of columnar

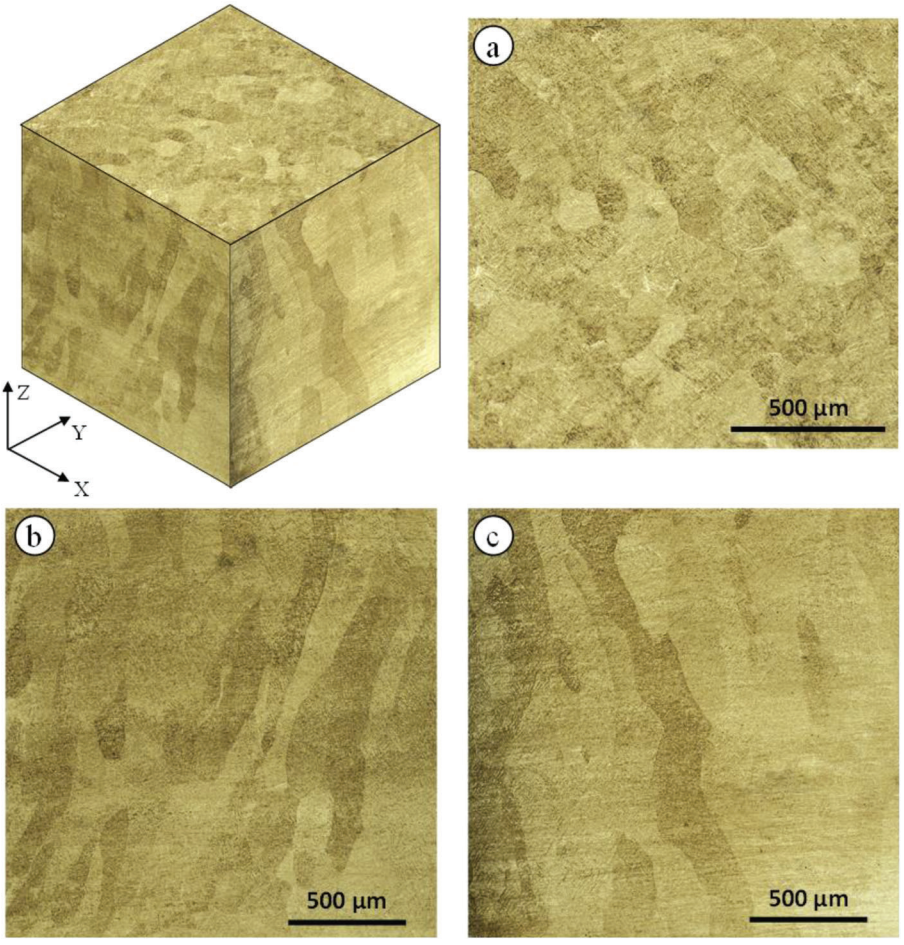

Figure 5. Macrostructure of columnar prior grains in different sections parallel and perpendicular to the LENS build direction (Z axis) (a) XY plane, (b) XZ plane, (c) YZ plane.

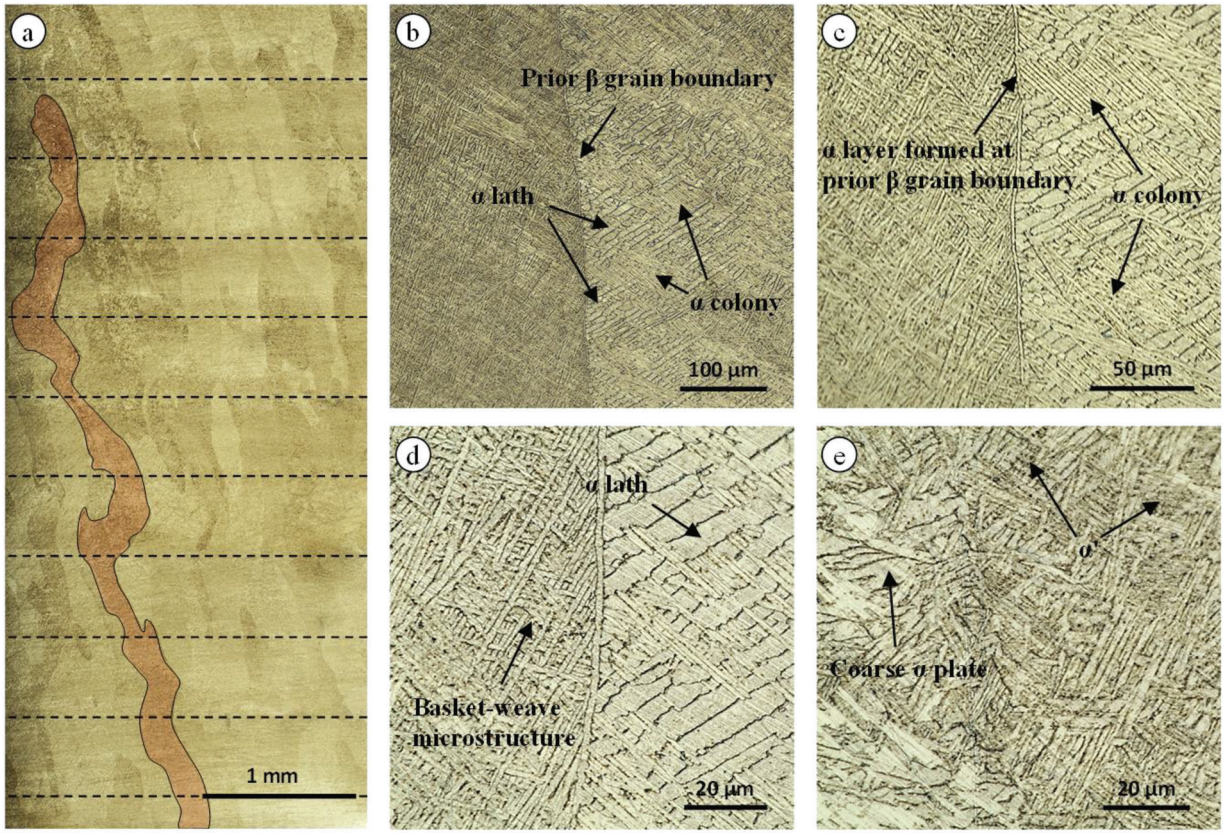

Figure 6. a) representative illustration of a prior β grain growing through several sintered layers along the build direction in LENS samples, (b–d) different magnifications of the microstructure of LENS samples illustrating the area between two prior β grains, (e) acicular α' microstructure of LENS samples.

and basket-weave $\alpha + \beta$ grains and acicular α'. The microstructure of wrought Ti-6Al-4V alloy at different magnifications is shown in **Figure 7**. According to Figure 7, the microstructure of wrought samples includes lighter equiaxed α grains with an average grain size of 5 μm surrounded with darker β phase. The microstructural features of both studied materials were evaluated in more details using SEM analysis. **Figure 8** illustrates various microstructures revealed under SEM. The Al-reach black zones in Figure 8 correspond to α and α' phases, while the white zones, reach in vanadium, correspond to β phase.

3.2. Fatigue Strength and Notch Sensitivity

The results obtained from the statistical elaboration of fatigue test data for different specimen geometries made of LENS and

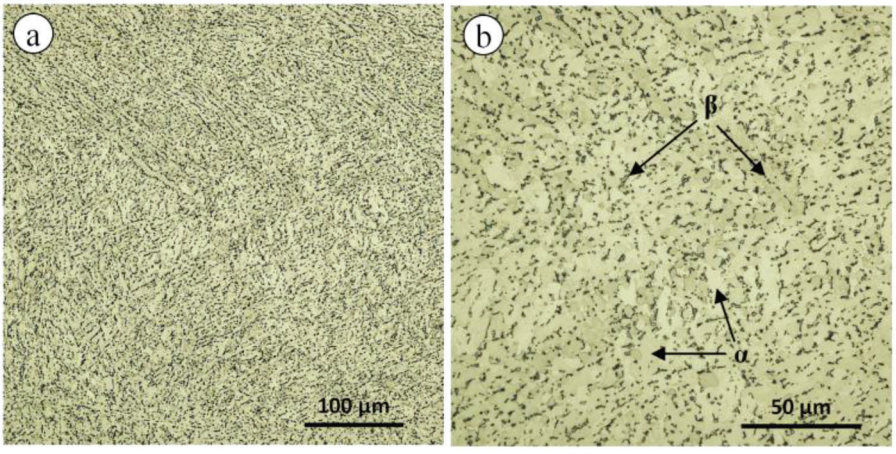

Figure 7. Microstructure of the wrought Ti-6Al-4V samples at different magnifications showing α and β phases (a) low magnification, (b) high magnification.

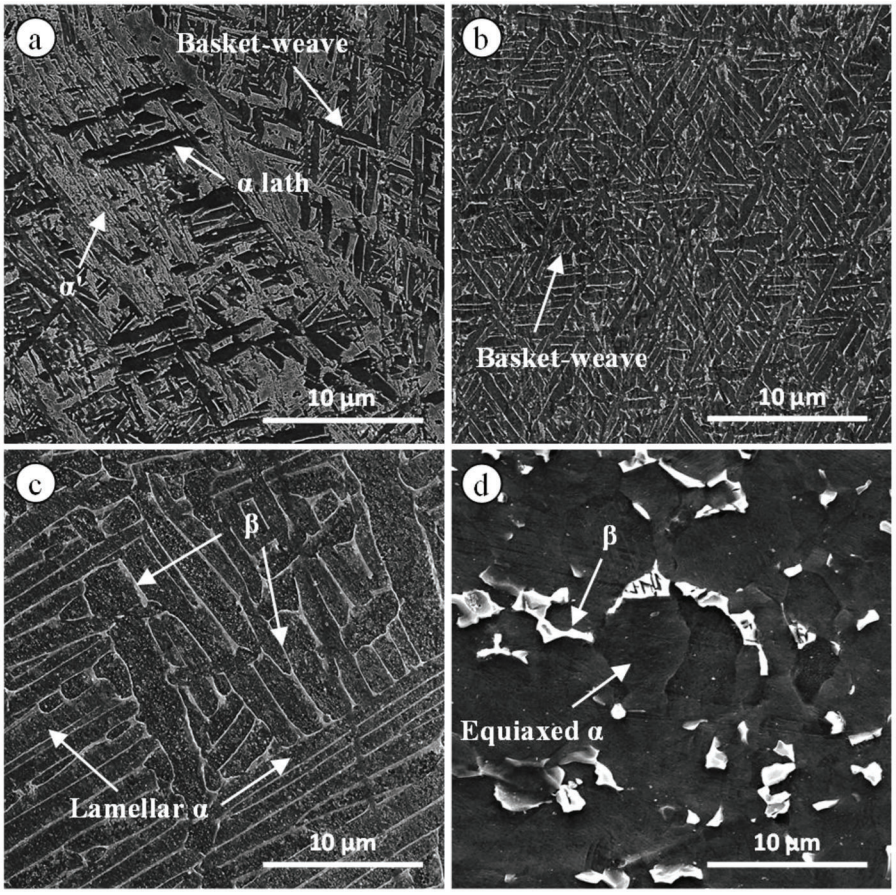

Figure 8. SEM illustration of (a–c) different phases observed in LENS) and (d) wrought samples.

wrought Ti-6Al-4V are reported in **Figures 9** and **10**, respectively. The fatigue strength of smooth, semi-circular notch and V-notch specimens made by LENS process at 10^6 cycles were 482, 477, and 293 MPa. While in the case of wrought specimens, fatigue strengths of 345, 344, and 258 MPa were obtained for smooth, semi-circular notch and V-notch specimens. In both cases, as expected the fatigue strength was reduced in presence of notches having the lowest value for V-notched specimens. According to the fatigue data illustrated in Figure 9 and 10, while the scatter index, T_σ of the smooth and semi-circular specimens is approximately the same, the V-notch specimens had slightly higher scatter bands. The detailed fatigue data of all the tested specimens together with stress concentration factor and notch reduction factor of each tested case are presented in **Table 2**. According to Table 2, lower fatigue notch factors were obtained for the semi-circular and V-notched specimens made of wrought Ti-6Al-4V compared to the LENS notched specimens which has resulted in lower notch sensitivity of wrought material compared to the LENS fabricated material. The notch sensitivities of both studied materials were higher when V-notch geometry was introduced in the specimen.

3.3. Fractography

SEM fractographs of the tested specimens are shown in **Figures 11** and **12**. It should be noted that since the LENS samples were machined to get the final geometry of the test specimens, the surface of the tested specimens is not that of the original build. According to Figure 11, the fracture surface of LENS specimens represents a flaky appearance at the vicinity of fatigue nucleation site. Getting farther from the initiation site, the surface features appear to be blockier in nature until reaching the final inclined fracture surface which is characterized by dimples showing the ductile nature of failure by void coalescence in the final stage of the crack propagation.

Unlike the LENS specimens, all wrought specimens experienced uniform fatigue crack nucleation from specimen surface (see Figure 12). The fracture in the wrought specimens do not show a clear flaky fatigue crack growth appearance, having a more uniform fatigue fracture surface from the initiation point up to the final failure.

3.4. Theoretical Fatigue Assessment Results

Linear elastic analyses were performed on different specimen geometries to obtain the ASED value. Critical radii of $R_0 = 0.366$ mm and 0.538 mm were calculated respectively for LENS and wrought materials using the formulation given in section 2.4. The results of ASED analysis with confidence bands of 10%, 50%, and 90% are presented in **Figure 13**. All the analyzed data are presented in a scatter band of $T_W = 2.07$ and inverse slope of

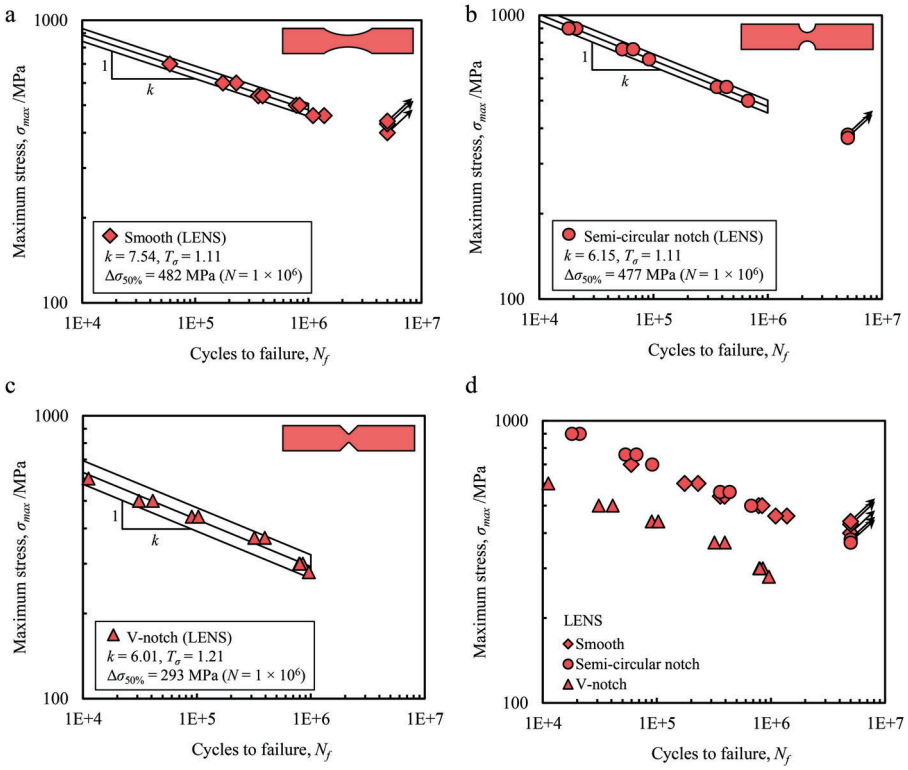

Figure 9. Fatigue data from different specimen geometries made by LENS process tested under loading ratio of $R = 0.01$ and 10 Hz loading frequency: (a) smooth,[25] (b) semi-circular notch, (c) V-notch, (d) comparative presentation of all geometries.

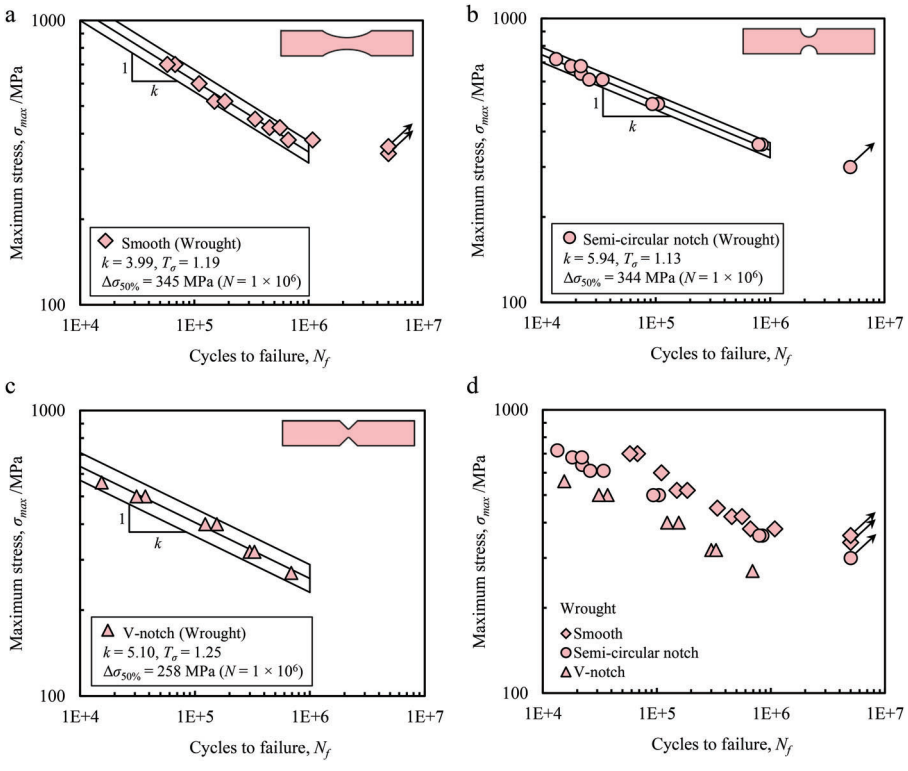

Figure 10. Fatigue data from different specimen geometries made of wrought Ti-6Al-4V tested under loading ratio of $R = 0.01$ and 10 Hz loading frequency: (a) smooth,[25] (b) semi-circular notch, (c) V-notch, (d) comparative presentation of all geometries.

Table 2. Fatigue behavior of the tested Ti-6Al-4V specimens.

Material	Geometry	$\Delta\sigma_{50\%}$[a)] [MPa]	T_σ	k	K_t	K_f	q
LENS	Smooth	482	1.11	7.54	1.073	–	–
	Semi-circular notch	477	1.11	6.15	1.308	1.010	0.03
	V-notch	293	1.20	6.05	2.279	1.645	0.50
Wrought	Smooth	345	1.19	3.99	1.073	–	–
	Semi-circular notch	344	1.13	5.94	1.308	1.003	0.01
	V-notch	258	1.25	5.10	2.279	1.337	0.26

[a)] Fatigue strength at 1×10^6 cycles.

$k = 2.53$ for LENS specimens and $T_W = 1.63$ and $k = 2.63$ for wrought specimens. The obtained scatter bands have reasonably small values compared to the values reported in the open literature for steel notched components.[40,41]

4. Discussion

Fatigue behavior of LENS Ti-6Al-4V specimens in presence of geometrical discontinuities has been evaluated in this study. The fatigue limits of different specimen geometries were experimentally obtained and used for notch sensitivity analysis. Different fatigue behavior and fatigue failure mechanisms of the two studied materials were corelated to the difference in their microstructures. Due to lack of fabrication faults in the machined LENS specimens, the main governing factor for defining the failure of these components is assumed to be the microstructure of the material and induced notches in the specimens.

4.1. Microstructure

According to the microstructure of LENS samples (see Figures 5 and 6), as a result of sequential layer deposition an epitaxial grain growth through the height of the sample occurs during the LENS process, leading to a columnar prior-β grain structure. Although a layer height of 0.508 mm was used for fabrication of the LENS samples, the columnar grains grew over several sintered layers (see Figure 6a) having 0.2–0.3 mm width. Since the melting temperature is commonly in a range higher than transus temperature, the solidified sintered metal forms β phase which

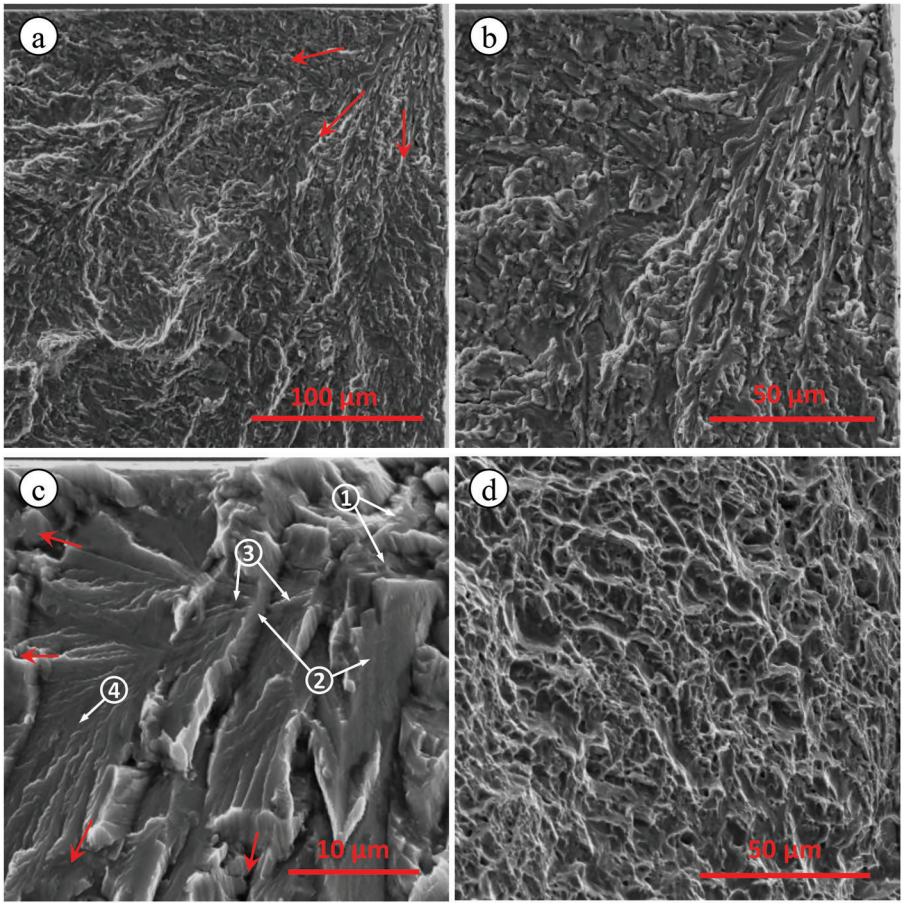

Figure 11. SEM fractograph of the tested LENS specimens; (a,b) fatigue fracture surface, (c) localized fatigue initiation site within the material, the numbers indicate: 1) fatigue initiation site, 2) intergranular failure (on the boundary of α lamellae), 3) transgranular crack growth through the α lamellae in the colony, 4) rivers formed due to crack propagation through a twist grain boundary, and (c) the ductile failure surface. (red arrows indicate the direction of fatigue crack propagation).

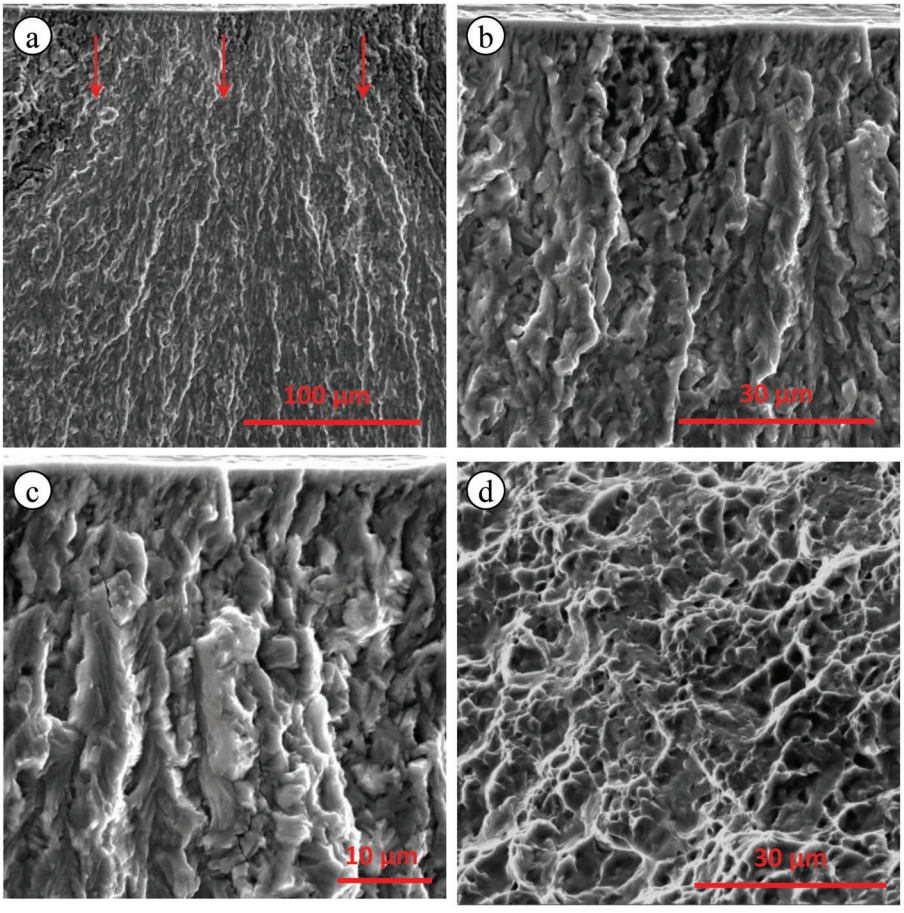

Figure 12. SEM fractograph of the tested wrought specimens; (a,b) fatigue fracture surface, (c) uniform fatigue initiation from the specimen's edge and (c) the ductile failure surface. (red arrows indicate the direction of fatigue crack propagation).

subsequently transforms during cooling and re-heating of the bottom layers. Nucleation of α phase within the prior β grains leads to formation of a basketweave structure by transformation of β phase into a martensitic type of α phase, namely α'. The acicular α' martensite phase induced by the high cooling rate, describes the lower ductility of the LENS samples compared to the conventionally made titanium alloy.[18] According to Figures 6 and 7, very fine α' grains of length 5–10 μm and width of ≈0.3 μm were observed within the columnar prior-β grains. These observations are consistent with the previous researches in the literature, where presence of α' martensite phase within a prior-β grain parallel to the deposit building direction was reported.[12,14,18,34,37]

Unlike powder bed AM methods, where the heat induced by sintering can be transferred through both the surrounding powder and the specimens itself, the induced heat during DED

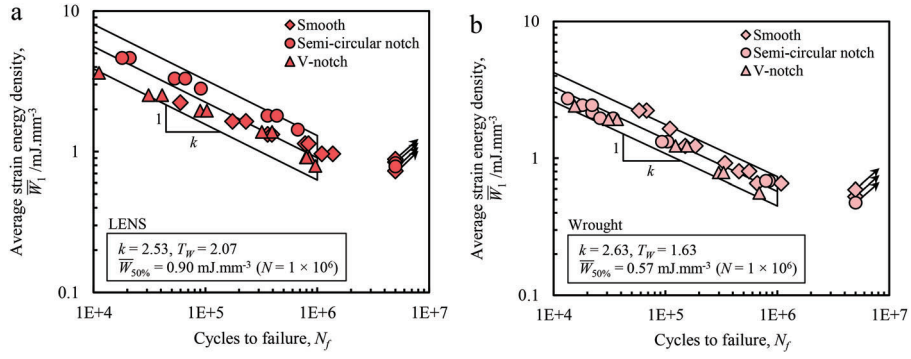

Figure 13. Synthesis of fatigue data based on SED; (a) LENS specimens, (b) wrought specimens.

process transfer through the sintered layers, reheating them and possibly resulting in partial α′-α transformation. In this case, α colonies start to form close to the prior-β grain boundaries. On the other hand, Qiu et al.[49] reported that performing stress-relief heat treatment induces α′-α transformation. This phase transformation is thought to be partially occurred also in the LENS samples analyzed in the current work after the stress-relief heat treatment. It is worth mentioning that the microstructure of LENS parts is strongly dependent on the thermal history during the fabrication process. Hence, predicting the microstructural characteristics of LENS parts and the level of their dependence on the process parameters is still to be studied.[17] Numerous researches have been conducted in the past to evaluate the effect of different process parameters on the microstructural features and material properties of LENS parts.[50–53]

4.2. Notch Sensitivity and Failure Mechanisms

Dealing with titanium alloys with Hexagonal Close Packed (HCP) α and Body Central Cubic (BCC) β crystal lattice characteristics, the fatigue behavior highly depends on the morphology and size of the α phase in the material.[12,54] As a result of finer α grain size of LENS samples, higher high cycle fatigue strength can be obtained for this material.[13]

Considering the lattice structure of HCP α phase, only limited number of slip system occurs within this phase which are all parallel to each other (planes (0001) in Miller-Bravais system). This limited number of slip system compared to Cubic Crustal (CC) structures, reduces the chance of moving mobile dislocations in favorable planes resulting in lower likelihood of formation of intrusions and extrusion, which are the leading cause of crack initiation in the material.[54] In this scenario, several potential crack initiation sites can arise within the reduced section of a smooth specimen. While, in the case of the notched specimens with smaller reduced volume (i.e., the length of reduced section is shorter in notched specimens), there is a lower possibility of formation of intrusions and extrusions. Among the studied geometries, V-notched specimens have the lowest possibility of formation of intrusions and extrusions, making these specimens more resistant to fatigue if the comparison is made based on the local notch stress. Depending on the presence of grains with favorable crystallographic orientation in the small region around the V-notch tip, the fatigue life can vary. This dependency of fatigue life of V-notched specimens to the microstructure, results in higher scatter band of the fatigue data for this geometry. As a result of high fatigue limit of notched specimens, lower notch sensitivity values are obtained for the tested wrought material. Dealing with LENS specimens with finer α grains, lower plastic yielding occurs in the notched region compared to the wrought notched specimens, increasing the notch sensitivity of the material in this case. It should be mentioned that the notch sensitivity is rather a combined material-geometrical factor that for a constant material can changed by changing the geometry of the notch. However, as a general term, this parameter is being used by engineers and scientists to compare the notch fatigue behavior of different materials.

Complex fatigue crack initiation mechanism with multiple crack propagation directions from the initiation site was observed in the LENS specimens. According to Figure 11c, cross-colony slip-band crack initiation was observed for LENS specimens, with subsequent small-crack growth generally occurring along the planar-slip bands into neighboring, but differently oriented, lamellar colonies. In these specimens, the crystallographic crack initiation and propagation favored by aligned α lamellar colonies is expected. The fatigue crack cut across the α lamellae which have the main axes aligned almost parallel to the stress axis (i.e. transgranular failure). On the other hand, if the α lamellae are oriented perpendicular to the load axis, intergranular crack growth along the lamellae boundaries occurs (see Figure 11). The fatigue crack initiation

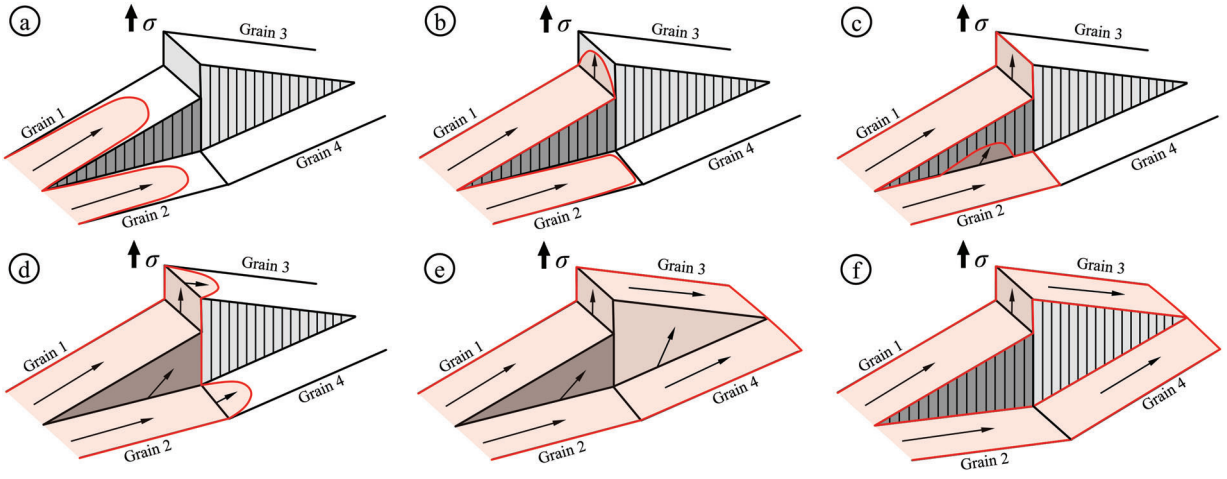

Figure 14. Schematic illustration of fatigue crack growth in Ti-6Al-4V. a) formation of a rough crack front geometry in two adjacent grains (grain 1 and grain 2); (b) intergranular crack propagation between grain 1 and 3; (c) crack growth along unfavored crack path (the step between grain 1 and 3); (d) crack growth with different angle according to the grain orientation in grain 3 and 4; (e) rejoining of the cracks in grain 3 and 4; (f) rejoining of the separate cracks without any crack propagation in the hatched area, as a result of retarded crack in this region due to large step height (the uncracked hatched area in this case is called bridging ligament).

Table 3. Synthesis of the experimental results of smooth and V-notch specimens by ASED.

Material	W versus N_f relationship	T_σ	T_W	R_0 [mm]
LENS	$\overline{W} = 67.02N_f^{-0.308}$	Smooth: 1.11 V-notch:1.21	1.42	0.366
Wrought	$\overline{W} = 181.04N_f^{-0.419}$	Smooth: 1.19 V-notch:1.25	1.90	0.538

in the wrought material is also somewhat influenced by the microstructure, but due to equiaxed microstructure of this material, typical fatigue crack initiation from the specimen edge was observed with significantly lower tortuosity (see Figure 12). The microstructural fatigue crack propagation is schematically illustrated in **Figure 14**. According to fractography results, the fatigue crack splits into separate, crystallographically favorable oriented crack planes in adjacent grains or colonies, leaving some steps between the fatigue crack growth facets (hatched area in Figure 14), the height of which is proportional to the grain or colony size.[55] Presence of these steps in the crack front geometry can effectively retard further extension of the crack to form again a continuous and uniform crack front (Figure 14b). This crack growth retardation is a result of forcing the crack to propagate along a crack path which is microstructurally unfavored in addition to the fact that the step plane has an unfavorable angle towards the stress axis (shown by σ in Figure 14). The schematic view of crack propagation through the step plane is shown in Figure 14b. It is worth mentioning that depending on the size of the steps, the retardation effect was reported by Peters et al.[56] to be so large that rejoining of the separated crack fronts by continuous growth and before crack growth in the step area can occur (through grain 1 to grain 3 and grain 2 to grain 4) resulting in un-cracked, so-called bridging ligaments (see Figure 14f). Due to presence of columnar prior β grains, and large lamellar microstructure and α colonies in LENS specimens, the height of the steps on the fracture surface was larger than that of wrought specimens with equiaxed α grains (Figures 11 and 12) contributing to a reasonably rougher fracture surface of LENS specimens and consequently more roughness induced closure effects during fatigue crack propagation.

4.3. Theoretical Analysis

Various key factors namely global geometrical discontinuities (i.e., notch and crack), local geometrical discontinuities (i.e., internal defects and surface roughness), microstructure, failure mechanism, and residual stress govern the fatigue failure of different mechanical structures. Hence, a practical way for fatigue assessment of these components would be to employ a general failure criterion that can take into account all these factors by use of a limited experimental information as input. The volumetric local approaches such as ASED are thought to count for the mentioned factors by the help of averaging all material inhomogeneities, resulting the criterion to be valid for the multiscale design of components.[40,41] The two different material production methods in this study resulted in different microstructures and failure mechanisms. Hence, two separate sets of theoretical analyses were performed on the test data to assess the notch fatigue behavior.

According to Figure 13, the agreement between the ASED results and experimental data was found to be satisfactory. By using the fatigue data in a range from 10^4 to 10^6 and considering the probabilities of survival Ps = 10% and 90%, energy-based scatter indexes, T_W of 2.07 and 1.63 were obtained for LENS and wrought materials. These scatter indexes become equal to 1.44 and 1.28 when reconverted to an equivalent local stress range with the same probability of survival ($T_\sigma = \sqrt{T_W}$), which is a reasonably small value compared to the stress-based curves in Figures 9 and 10.

According to ASED criterion, by performing experiments on two sets of specimens, i.e., smooth and sharp notched specimens, one can calculate the critical radius and obtain the fitting constants of the ASED-life formula as $\overline{W} = AN_f^B$. By performing the ASED analysis on both sets of fatigue data on LENS and wrought specimens, these ASED constants were obtained and reported in **Table 3**. These data can then be used to predict the fatigue behavior of other notched components made of the same materials. The obtained theoretical results for different geometries of the test specimens are summarized in the experimental, N_f, versus estimated, $N_{f,SED}$ fatigue life plots illustrated in **Figure 15** for both LENS and wrought materials. The fatigue predictions for wrought specimens are seen to fall always within the parent scatter band obtained from the

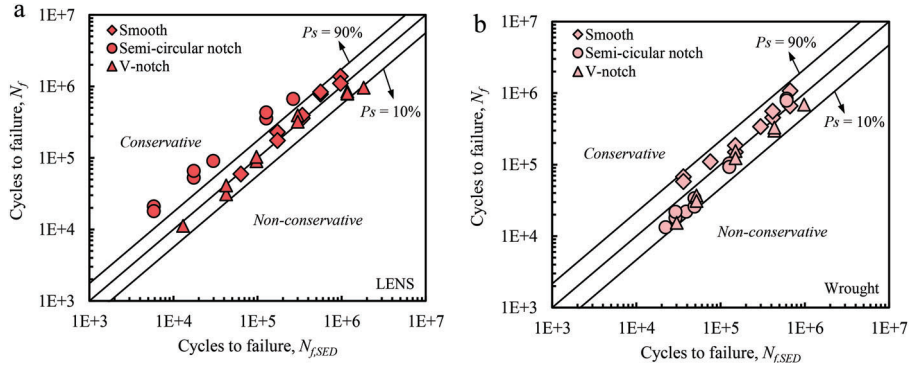

Figure 15. The accuracy of ASED criterion in predicting the fatigue life of the tested specimens; a) LENS, b) wrought. (The scatter bands with 10, 50, and 90% probability of survival were obtained from the test results of smooth and V-notch specimens).

reference specimens. however, the predictions for semi-circular notch specimens made by LENS process nearly fall outside of the parent scatter band but on the conservative side. This was consistent with the previous studies reporting conservative predations of semi-circular notched specimens when the ASED method was used.[57] To conclude, by considering the AM material as a new material, one can have an engineering prediction of fatigue life by use of the conventional fatigue criteria such as ASED method.

5. Conclusions

The major aim of this research was to investigate the effect of presence of geometrical discontinuities on the fatigue properties of additively manufactured Ti-6Al-4V, produced with LENS. The following conclusions can be drawn from the present investigation:

1) The microstructural analysis of LENS samples revealed presence of lamellar α, basket-weave α + β, α colonies, and very fine α' martensite phases within the columnar prior β grains. While for the wrought samples, coarse equiaxed α gains decorated with β grains were observed.
2) All the tested LENS specimens including smooth and notched specimens underwent higher number of cycles to failure compared to the cases were wrought material was tested. This enhanced fatigue strength was attributed to the finer grain size in LENS specimens resulting in higher fatigue nucleation life as well as presence of basket-weave and columnar prior β grains in the material resulting in higher degree of tortuosity and accordingly more roughness induced closure effects during crack propagation in LENS material. The fractographical analyses of the tested specimens revealed a cross-colony slip-band crack initiation mechanism for LENS specimens, while a mostly uniform fatigue crack initiation from the edge of specimens was observed for wrought specimens.
3) In the case of V-notched specimens, smaller reduced area ahead of notch tip was thought to lead to lower likelihood of presence of grains with favorable grain orientation for fatigue crack initiation in this region, which consequently resulted in higher scatter band of the fatigue data for this geometry compared to smooth specimens. On the other hand, larger reduced area in the notched region of semi-circular notched specimens resulted in almost similar probability of presence of favorable grain orientation for fatigue initiation in these specimens to the smooth specimens. Due to finer grains in LENS specimens, the lower plastic yielding in the notched region resulted in higher fatigue notch factor compared to wrought specimens.
4) Synthesis of fatigue data was performed by use of ASED criterion. The theoretical results showed a good consistency with the experimental data.

Conflict of Interest

The authors declare no conflict of interest.

Keywords

additive manufacturing, direct energy deposition, fatigue, notch, Ti-6Al-4V

Received: February 26, 2019
Revised: May 3, 2019
Published online:

[1] C. R. Deckard, *Method and Apparatus for Producing Parts by Selective Sintering*, **1989**, US4863538A.
[2] OPTOMEC, https://www.optomec.com/, accessed: February, **2019**.
[3] R. P. Mudge, N. R. Wald, *Weld. J. – New York* **2007**, *86*, 44.
[4] M. L. Griffith, D. M. Keicher, C. L. Atwood, J. A. Romero, J. E. Smugeresky, L. D. Harwell, D. L. Greene, *Proc. 7th Solid Free. Fabr. Symp*. **1996**, 125.
[5] M. L. Griffith, M. T. Ensz, J. D. Puskar, C. V. Robino, J. A. Brooks, J. A. Philliber, J. E. Smugeresky, W. H. Hofmeister *MRS Proc.*, **2000**, *625*, 9.
[6] G. K. Lewis, E. Schlienger, *Mater. Des*. **2000**, *21*, 417.
[7] A. Bandyopadhyay, B. V. Krishna, W. Xue, S. Bose, *J. Mater. Sci. Mater. Med*. **2009**, *20*, S29.
[8] D. G. Ahn, *Int. J. Precis. Eng. Manuf. – Green Technol*. **2016**, *3*, 381.
[9] R. Liu, Z. Wang, T. Sparks, F. Liou, J. Newkirk, *Aerospace Applications of Laser Additive Manufacturing*, Elsevier Ltd., Sawston, Cambridge, UK **2016**, pp. 351–371.
[10] D. G. Ahn, *Int. J. Precis. Eng. Manuf*. **2013**, *14*, 1271.
[11] O. Oyelola, P. Crawforth, R. M'Saoubi, A. T. Clare, *Addit. Manuf*. **2018**, *19*, 39.
[12] Y. Zhai, D. A. Lados, E. J. Brown, G. N. Vigilante, *Int. J. Fatigue* **2016**, *93*, 51.
[13] A. J. Sterling, B. Torries, N. Shamsaei, S. M. Thompson, D. W. Seely, *Mater. Sci. Eng. A* **2016**, *655*, 100.
[14] H. R. Sandgren, Y. Zhai, D. A. Lados, P. A. Shade, J. C. Schuren, M. A. Groeber, P. Kenesei, A. G. Gavras, *Addit. Manuf*. **2016**, *12*, 132.
[15] S. Wolff, T. Lee, E. Faierson, K. Ehmann, J. Cao, *J. Manuf. Process*. **2016**, *24*, 397.
[16] N. A. Kistler, D. J. Corbin, A. R. Nassar, E. W. Reutzel, A. M. Beese, *J. Mater. Process. Technol*. **2019**, *264*, 172.
[17] N. Shamsaei, A. Yadollahi, L. Bian, S. M. Thompson, *Addit. Manuf*. **2015**, *8*, 12.
[18] A. Bagheri, N. Shamsaei, S. Thompson, A. Bagheri, N. Shamsaei, in *Int. Mech. Eng. Congr. Expo*., ASME, Houston, Texas **2015**.
[19] P. A. Kobryn, S. L. Semiatin, in *Proc. 12nd Solid Free Fabr*, Austin **2001**, 179.
[20] C. Selcuk, *Powder Metall*. **2011**, *54*, 94.
[21] S. Razavi, G. Bordonaro, P. Ferro, J. Torgersen, F. Berto, *Proc. Inst. Mech. Eng. Part C J. Mech. Eng. Sci*. **2018**. https://doi.org/10.1177/0954406218813384
[22] A. W. Prabhu, T. Vincent, A. Chaudhary, W. Zhang, S. S. Babu, *Sci. Technol. Weld. Join*. **2015**, *20*, 659.
[23] L. Bian, S. M. Thompson, N. Shamsaei, *Jom* **2015**, *67*, 629.
[24] E. Amsterdam, G. A. Kool, in *ICAF 2009, Bridg. Gap between Theory Oper. Pract*. Springer, Rotterdam **2009**, 1261.
[25] S. M. J. Razavi, G. G. Bordonaro, P. Ferro, J. Torgersen, F. Berto, *Materials* **2018**, *11*, 284.
[26] M. Kahlin, H. Ansell, J. J. Moverare, *Int. J. Fatigue* **2017**, *101*, 51.
[27] S. M. J. Razavi, P. Ferro, F. Berto, *Metals* **2017**, *7*, 291.
[28] S. M. J. Razavi, P. Ferro, F. Berto, J. Torgersen, *Theor. Appl. Fract. Mech*. **2018**, *97*, 376.
[29] K. Solberg, F. Berto, *Int. J. Fatigue* **2019**, *122*, 35.
[30] M. Benedetti, C. Santus, *Int. J. Fatigue* **2019**, *121*, 281.
[31] F. Berto, J. Razavi, *Mater. Des. Process. Commun*. **2019**, https://doi.org/10.1002/mdp2.27

[32] F. F. Schmidt, R. A. Wood, *Heat Treatment of Titanium and Titanium Alloys*, NASA TM X-53445, NASA Marshall Space Flight Center, Huntsville, AL, USA **1966**, p. 77.
[33] A. R. Nassar, J. S. Keist, E. W. Reutzel, T. J. Spurgeon, *Addit. Manuf.* **2015**, *6*, 39.
[34] Y. Zhai, H. Galarraga, D. A. Lados, *Procedia Eng.* **2015**, *114*, 658.
[35] S. J. Wolff, S. Lin, E. J. Faierson, W. K. Liu, G. J. Wagner, J. Cao, *Acta Mater.* **2017**, *132*, 106.
[36] M. Buciumeanu, A. Bagheri, N. Shamsaei, S. M. Thompson, F. S. Silva, B. Henriques, *Tribol. Int.* **2018**, *119*, 381.
[37] S. A. Niknam, D. Li, G. Das, *Int. J. Adv. Manuf. Technol.* **2019**, *100*, 1731.
[38] E. Santecchia, A. M. S. Hamouda, F. Musharavati, E. Zalnezhad, M. Cabibbo, M. El Mehtedi, S. Spigarelli, *Adv. Mater. Sci. Eng.* **2016**, *2016*, 1. https://doi.org/10.1155/2016/9573524
[39] D. Taylor, *Eng. Fract. Mech.* **2008**, *75*, 1696.
[40] F. Berto, P. Lazzarin, *Theor. Appl. Fract. Mech.* **2009**, *52*, 183.
[41] F. Berto, P. Lazzarin, *Mater. Sci. Eng. R* **2014**, *75*, 1.
[42] F. Berto, S. M. J. Razavi, J. Torgersen, *Frat. Ed Integrita Strutt.* **2018**, *12*, 1. https://doi.org/10.3221/IGF-ESIS.43.01
[43] E. Beltrami, *Nuovo Cim.* **1885**, *18*, 145.
[44] G. C. Sih, in *Mech. Fract.*, Noordhoff International Publishing, Leyden **1973**, 21.
[45] P. Lazzarin, R. Zambardi, *Int. J. Fract.* **2001**, *112*, 275.
[46] M. L. Williams, *J. Appl. Mech.* **1952**, *19*, 526.
[47] P. Lazzarin, F. Berto, *Int. J. Fract.* **2005**, *135*, 161.
[48] P. Lazzarin, T. Lassen, P. Livieri, *Fatigue Fract. Eng. Mater. Struct.* **2003**, *26*, 49.
[49] C. Qiu, N. J. E. Adkins, M. M. Attallah, *Mater. Sci. Eng. A* **2013**, *578*, 230.
[50] M. Griffith, M. Schlienger, L. Harwell, in *Solid Free. Fabr. Symp. Proc.*, University of Texas at Austin Publishers, Austin, TX **1998**, 89.
[51] S. Bontha, N. W. Klingbeil, P. A. Kobryn, H. L. Fraser, *J. Mater. Process. Technol.* **2006**, *178*, 135.
[52] B. Zheng, Y. Zhou, J. E. Smugeresky, J. M. Schoenung, E. J. Lavernia, *Metall. Mater. Trans. A* **2008**, *39*, 2228.
[53] S. Bontha, N. W. Klingbeil, P. A. Kobryn, H. L. Fraser, *Mater. Sci. Eng. A* **2009**, *513–514*, 311.
[54] S. Hosseini, in *Biomed. Eng. – Tech. Appl. Med.*, IntechOpen, London, UK **2012**, 75.
[55] G. Lütjering, A. Gysler, L. Wagner, in *Proc. The 6th World Conference on Titanium* (Eds: P. Lacombe, R. Tricot, G. Beranger), Les Editions de Physiques, Les Ulis **1988**, 71.
[56] J. O. Peters, E. Janvier, G. Lütjering, in *Proc. Fatigue* **2002** (Ed: A. F. Blom), EMAS, Stockholm **2002**, 1805.
[57] Z. Hu, F. Berto, Y. Hong, L. Susmel, *Int. J. Fatigue* **2019**, *123*, 105.